Int J Adv Manuf Technol (2005) 25: 833–840
DOI 10.1007/s00170-003-1930-5

ORIGINAL ARTICLE

Tae-Sung Jung · Min-Yang Yang · Kang-Jae Lee

A new approach to analysing machined surfaces by ball-end milling, part I:

Formulation of characteristic lines of cut remainder

Received: 22 April 2003 / Accepted: 23 August 2003 / Published online: 16 March 2004

Abstract Since productivity and product quality are always regarded as important issues in manufacturing technologies, a reliable method for predicting machining errors is essential to meeting these two conflicting requirements. However, the conventional roughness model is not suitable for the evaluation of machining errors for highly efficient machining conditions. Therefore, a different approach is needed for a more accurate calculation of machining errors. This study deals with the geometrical surface roughness in ball-end milling. In this work, a new method, called the *ridge method*, is proposed for the prediction of the machined surface roughness in the ball-end milling process. In Part I of this two-part paper, a theoretical analysis for the prediction of the characteristic lines of the cut remainder are generated from a surface generation mechanism of a ball-end milling process, and three types of ridges are defined. The trochoidal trajectories of cutting edges are considered in the evaluation of the cut remainder. The predicted results are compared with the results of a conventional roughness model.

Keywords Ball-end mill · Characteristic line (ridge) · Cut remainder · Surface roughness

1 Introduction

Today, sculptured surfaces are widely used for the design of complex products in the die/mould and aerospace industries. Ball-end milling is one of the most common manufacturing processes for these free-form surfaces.

Generally, unwanted machining results are introduced by a number of sources such as the deflection of tool-work system, chatter, tool wear, built-up edge, chip flow and the thermal effect of the cutting process [1–5]. Of these, the cutting forces are considered important causes of machining errors, and the effects of cutter deflection on the machined surface errors have been studied by many researchers [6–13].

However, the determination of cutting parameters such as step size and feedrate is usually based on a theoretical surface roughness. Since optimal machining conditions are essential for high productivity and product quality, it is necessary to predict more accurately the geometrical machining errors in ball-end milling. The geometrical roughness produced by a milling processes is normally approximated to a typical scallop profile. In many studies [14–16], the profiles of the scallop heights have been analysed for accurate tool path generation and given as a function of tool radii, path intervals and curvatures of machined surfaces, etc.

As the feedrate increases in an highly efficient machining condition, the roughness along the feed direction becomes a no longer negligible factor. However, only a few researchers have focused their attention on cutter mark height. Miyazawa and Takada [17] analysed the geometrical surface roughness when a curved surface is machined by a ball-end mill and suggested the micro-milling process. Later, Naito and co-workers [18] carried out an experiment to find a high-efficiency machining strategy in which the feed per tooth is made equal to the pickfeed to obtain a fine finish in plane surface machining. Kim and Chu [19, 20] studied the effects of cutter marks and run-out and predicted the machined surface texture by the superposition of the cutter marks and the conventional scallop surface. For a more exact prediction of the geometrical machining error, Koreta and Egawa [21] investigated the topologies of machined surfaces for highly efficient cutting conditions by simulating the envelopes of the cutting edges employing the conventional Z-map method. It has been noted in their work that the surface roughness for high-efficiency machining conditions cannot be evaluated by the conventional roughness model. Although the final shapes and roughness of resultant surface can be precisely estimated by the Z-map method, the simulation process unfortunately requires a vast amount of computationally intensive Boolean operations. So it is difficult to analyse explicitly the effects of various cutting parameters such as feedrate, pickfeed, tool geometry, cutting configuration, etc. on geometrical

T.-S. Jung · M.-Y. Yang (✉) · K.-J. Lee
Department of Mechanical Engineering,
Korea Advanced Institute of Science & Technology,
Daejeon, 305-701, South Korea
E-mail: myyang@kaist.ac.kr

roughness. Therefore, as an alternative to the simulation method, the formulation of an analytic form for the prediction of surface roughness in ball-end milling is helpful for machining condition optimisation.

This work puts strong emphasis on the prediction of the geometrical surface roughness produced by the ball-end milling process. A new method, called the *ridge method*, is proposed for evaluating the surface roughness. In Part I of this two-part paper, the characteristic lines of cut remainder are defined as *ridges* and their mathematical equations are derived from the surface generation mechanism of the ball-end milling process. Also, the conventional roughness models are briefly investigated with respect to the concept of ridges.

2 Methods for prediction of surface roughness

2.1 Spherical-tool approximation model

The surface roughness of machined surfaces is traditionally predicted by the *spherical-tool approximation model*. In this model, the envelope of the cutting edge is approximated to a hemisphere on the assumption that the spindle speed is considerably faster than the feedrate. As shown in Fig. 1a, the final topology of a machined surface is estimated by the superposition of the semi-spherical machined surfaces which are separated by as much as the feed per tooth and the path interval [17, 20].

Furthermore, the maximum surface roughness, $H_{\max}$, is simply calculated by summing the scallop heights and the cutter marks. Therefore, the theoretical roughness in plane cutting mode can be obtained by

$$H_{\max} = H_{\max,scallop} + H_{\max,cuttermark} = \frac{f_p^2}{8R} + \frac{f_t^2}{8R}\,, \tag{1}$$

where R, f_t and f_p denote the cutter radius, the feed per tooth and the path interval, respectively.

Figure 1b presents the characteristic line of the cut remainder, predicted by the conventional roughness model, which represents the trajectory of the peaks of the cut remainder.

In the conventional roughness model, the ridge is part of the circle with a radius of R' and exists in the *maximum cut remainder section*, Π. The equation for R' can be written as follows:

$$R' = \sqrt{R^2 - \left(\frac{f_t}{2}\right)^2}\,. \tag{2}$$

As shown in Fig. 1a, the maximum cut remainder section, Π is parallel to the common plane (XZ plane) and is also perpendicular to the feed direction, Y. Here, O–XYZ are the coordinates on the surface machined by any arbitrary cutting path. Furthermore, the ridge is symmetrical to the osculating plane

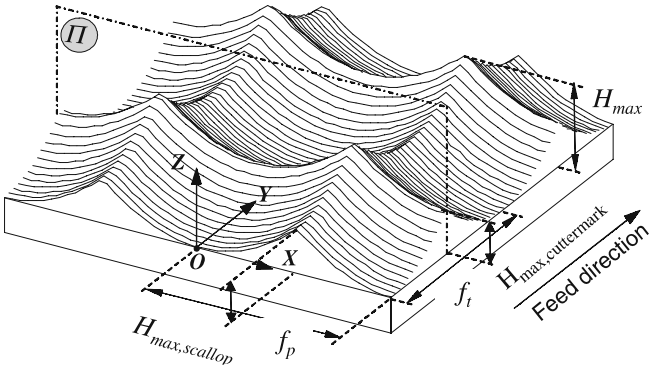

(a) Surface topology predicted by conventional roughness model

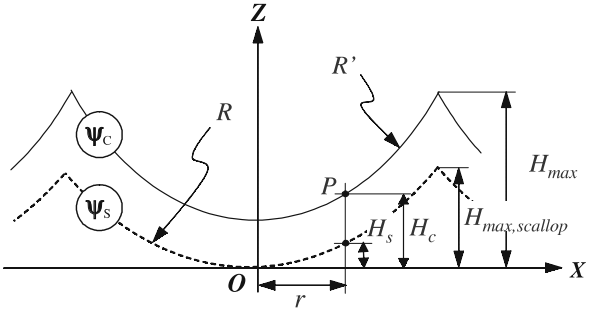

(b) Characteristic line of cut remainder (Ridge)

Fig. 1. Analysis of machined surface by spherical-tool approximation model

(YZ plane) in this roughness model. Hence the height of any arbitrary point P on the ridge H_C is obtained by

$$H_C = R - \sqrt{R'^2 - r^2} = R - \sqrt{R^2 - R_{eff,C}^2} \quad \text{for} \quad 0 \leqslant r \leqslant \frac{f_p}{2}\,, \tag{3}$$

where r is the radius of a cutting edge as shown in Fig. 1b, and subscript C represents the values predicted by the conventional roughness model.

From Eqs. 2 and 3 the *effective cutter radius*, $R_{eff,C}$, can be written as

$$R_{eff,C} = \frac{f_t}{2}\sqrt{1 + \left(\frac{2r}{f_t}\right)^2}\,. \tag{4}$$

Equation 4 can be rewritten as follows:

$$\tau_{\mathrm{R}eff,C} = \frac{R_{eff,C}}{f_t} = \frac{1}{2}\sqrt{1 + (2\tau_r)^2}\,, \tag{5}$$

where the *effective cutter radius ratio*, $\tau_{\mathrm{R}eff}$, is the ratio of effective cutter radius to the feed per tooth, R_{eff}/f_t, and τ_r is the ratio that represents r/f_t.

Finally, the trajectory of the ridge of the conventional roughness model, ψ_C, can be expressed as follows:

$$\psi_C = \begin{bmatrix} x_C \\ z_C \end{bmatrix} = \begin{bmatrix} \pm r \\ H_C \end{bmatrix}, \tag{6}$$

where $H_C = R - \sqrt{R^2 - R_{eff,C}^2}$.

In addition, the height of the scallop profile generated by the cutting edge of which the radius is r; H_S can be calculated by

$$H_S = R - \sqrt{R^2 - r^2} = R - \sqrt{R^2 - R_{eff,S}^2} \quad \text{for} \quad 0 \le r \le \frac{f_p}{2}, \tag{7}$$

where subscript S denotes the values corresponding to the scallop profile.

Hence the relationships between $\tau_{\mathrm{R}eff,S}$ and τ_r can be written as follows:

$$\tau_{\mathrm{R}eff,S} = \frac{R_{eff,S}}{f_t} = \tau_r \,. \tag{8}$$

2.2 Disk-tool approximation model

Commonly, the geometrical surface roughness and the final surface texture of ball-end milling are evaluated by the spherical-tool approximation model due to its simplicity of calculation. When the machining is performed under the condition where the feed per tooth is several times smaller than the path interval, the maximum surface roughness estimated by the conventional roughness model makes good agreement with that of the actual machined surface.

Recently, a machining strategy equalising the feed per tooth and the path interval has been adopted to obtain the checkerboard-shape machined surface known for more efficient path planning with respect to both machining and manual polishing time. It has also been found that the conventional roughness model is inappropriate for the evaluation of surface roughness under a high-efficiency machining condition. In previous research [21], the cutting simulation was performed with consideration of the actual trochoid paths of cutting edges based on the *disk-tool approximation model*, and it has been observed that the height of the cut remainder formed in the vicinity of the rotational centre of the tool is generally larger than the conventional cusp height.

In general, the cutting edges of the ball-end mill are composed of flutes with helix angles which vary locally in the ball part of the cutter. However, the helix angles of the flutes can be negligible because the depth of cut is very small in a finish cut, and a cutter with two flutes is commonly used. Thus its profiles can be approximated to the edges of a half-disc-shaped plane, Γ, as shown in Fig. 2a. In this work the plane, Γ, is referred to as the *cutting-edge plane*.

The disk-tool approximation model is one of the mathematical models used for the analysis of milling operations and is mainly related to the accurate calculation of the uncut chip thickness for the prediction of cutting forces. In this model, both the translational movement and the rotational movement of the cutting edges are considered differently from in the conventional roughness model, and the three-dimensional trajectory of the point P on the cutting edge can be expressed by

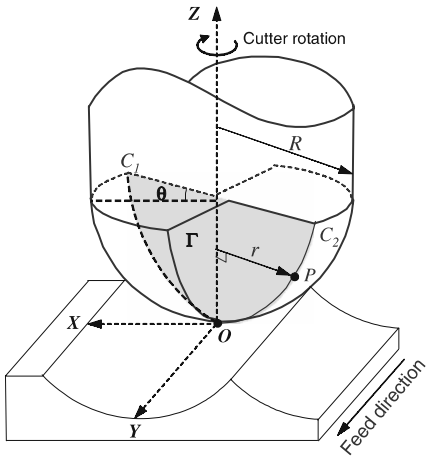

(a) Coordinate system of Disk-tool approximation model

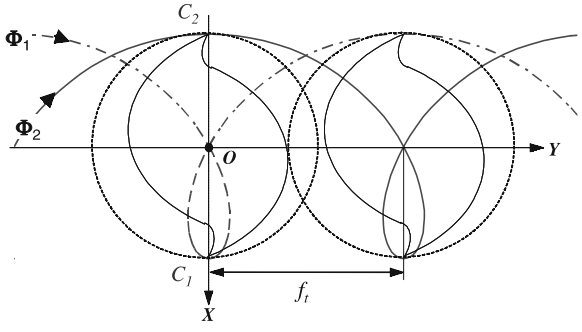

(b) Trochoidal trajectories of cutting edges

Fig. 2. Analysis of ball-end milling process

$$\Phi_n = \begin{bmatrix} r\cos(\theta - (n-1)\pi) \\ -r\sin(\theta - (n-1)\pi) \\ R - \sqrt{R^2 - r^2} \end{bmatrix} + \begin{bmatrix} 0 \\ f_t\left(\frac{\theta}{\pi}\right) \\ 0 \end{bmatrix}$$
$$\text{for } 0 \le r \le R \text{ and } n = 1, 2\,, \tag{9}$$

where subscript n represents the cutting edges C_1 and C_2 and θ is the rotation angle of the cutter measured from $+X$ axis, CW.

Figure 2b shows the trochoid paths of the cutting edge expressed by Eq. 9. As apparent from Fig. 2b, the regions where the trajectories of the cutting edges do not overlap each other remain as the cut remainder. Hence the height of the cut remainder in the right plane of the machined surface is larger than that in the left plane in the plane cutting mode.

The cut remainder is consequently determined by the relationship of the radius of the cutting edge and the feed per tooth. The geometrical cut remainder also increases as the radius of cutting edge becomes relatively smaller than the feedrate.

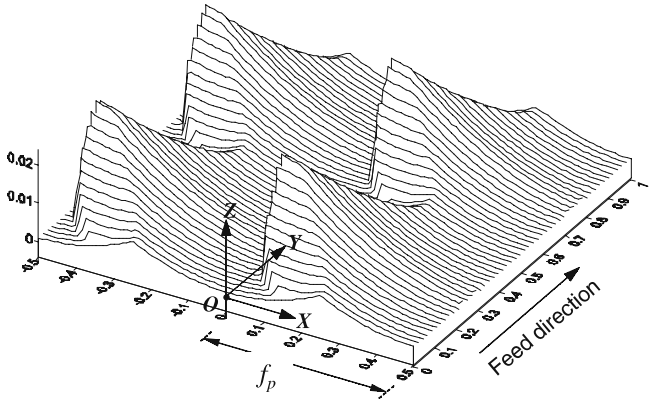

(a) Surface topology predicted by Z-map simulation

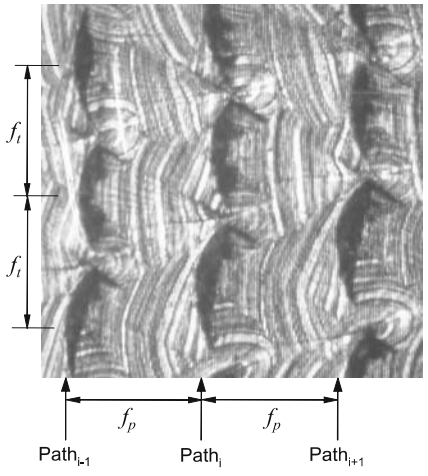

(b) Photograph of actual machined surface (top view)

Fig. 3. Analysis of machined surface by disk-tool approximation model

Figure 3a presents the predicted topography of the machined surface under the following cutting condition: a tool radius of 5 mm, a feed per tooth of 0.5 mm/tooth and a path interval of 0.5 mm. Figure 3b shows the actual machined surface under the same condition. Compared with the previous expectation in Fig. 1a, it differs noticeably in Fig. 3a. The maximum roughness expected by the Z-map method is 25 μm, which is twice the value of 12.5 μm calculated by Eq. 1.

3 Theoretical analysis of ridges

3.1 Surface generation mechanism of ball-end milling

To predict the surface roughness of ball-end milling more easily and accurately, the characteristic lines of surface texture are analysed based on the disk-tool approximation model in this study.

In the milling process, the final shapes of machined surfaces are generated by the superposition of the topographies created by adjacent cutting paths. Thus an understanding of the texture machined by a single cutting path aids in the prediction of the resultant surface.

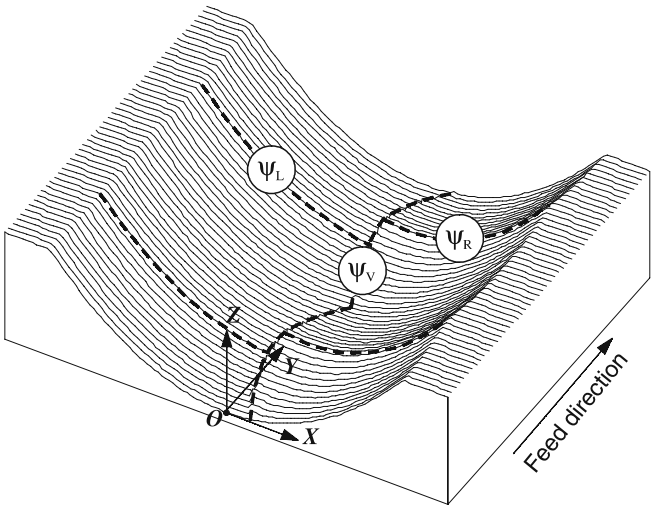

Fig. 4. Surface texture and ridges generated by single cutting path

Figure 4 shows the surface topology and the characteristic lines of the cut remainder generated by a single cutting path predicted by employing the disk-tool approximation model. As mentioned above, the ridge in the conventional roughness model is assumed to be part of the circle contained in the maximum cut remainder section, Π. However, the ridges in the disk-tool approximation model are classified into three types, as shown in Fig. 4. In this study, each of the ridges is defined as the *left ridge* (ψ_L), the *right ridge* (ψ_R) and the *critical-velocity ridge* (ψ_V), respectively, from a consideration of their positions and generation mechanisms. The left ridge and the right ridge exist in the maximum cut remainder section as in conventional roughness models. However, the critical-velocity ridge appears continuously along the feed direction in the right plane of the machined surface.

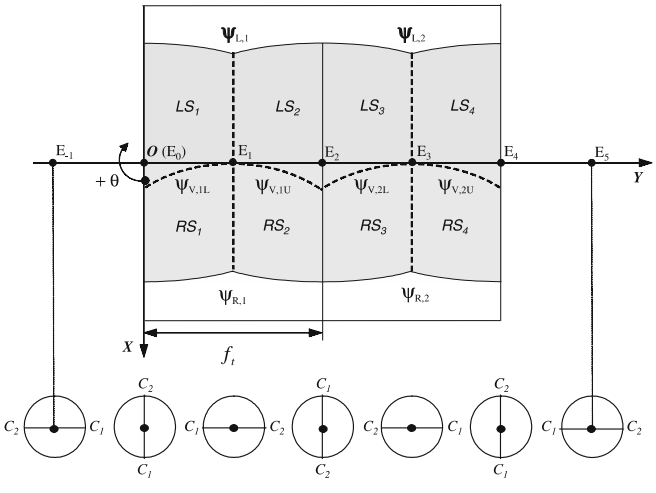

Fig. 5. Surface generation sequence of ball-end milling process (top view)

Table 1. Sequence of surface generation

Rotation angle (θ)	Tool center position	Cutting edge C_1	Cutting edge C_2
$[-\pi/2 \sim 0]$	$[E_{-1} \sim E_0]$	Generate machined surface RS_1	
$[0 \sim \pi/2]$	$[E_0 \sim E_1]$	Generate ridge $\psi_{V,1L}$	Generate machined surface LS_1
$[\pi/2 \sim \pi]$	$[E_1 \sim E_2]$	Generate machined surface LS_2 Generate ridge $\psi_{L,1}$	Generate machined surface RS_3 Generate ridge $\psi_{V,1U}$
$[\pi \sim 3\pi/2]$	$[E_2 \sim E_3]$	Generate machined surface LS_3	Generate machined surface RS_2 Generate ridge $\psi_{V,2L}$, $\psi_{R,1}$
$[3\pi/2 \sim 2\pi]$	$[E_3 \sim E_4]$	Generate ridge $\psi_{V,2U}$	Generate machined surface LS_4 Generate ridge $\psi_{L,2}$
$[2\pi \sim 5\pi/2]$	$[E_4 \sim E_5]$	Generate machined surface RS_4 Generate ridge $\psi_{R,2}$	

Figure 5 illustrates the surfaces and the ridges formed by the rotational movements of the cutting edges during the movement of the centre position of the cutter. The sequence of surface generation is summarised in Table 1.

3.2 Analytic presentation of ridges

3.2.1 Left ridge (ψ_L)

The first left ridge, $\psi_{L,1}$, is the intersection line of the machined surfaces, LS_1 and LS_2, in Fig. 5. As described in Table 1, the machined surface, LS_1, is generated by the cutting edge C_2 as the centre of the cutter moves from E_0 to E_1. Similarly, LS_2 is formed by the cutting edge C_1 as the tool moves from E_1 to E_2.

From the geometrical condition described above the generation mechanism of $\psi_{L,1}$ can be schematised as shown in Fig. 6a. From Fig. 6a the geometrical constraints at the arbitrary point $P(x_p, y_p, z_p)$ on $\psi_{L,1}$ can be represented mathematically as follows:

$$x_p = r_1 Sin\phi_1 = r_2 Sin\phi_2$$
$$z_p = R - \sqrt{R^2 - r_1^2} = R - \sqrt{R^2 - r_2^2}, \tag{10}$$

where r_1 and r_2 are the radii of cutting edges C_2 and C_1 acting on P.

From the equations above, the relationships between $r_1 - r_2$ and $\phi_1 - \phi_2$ are written as follows:

$$R_{eff,L} = r_1 = r_2$$
$$\phi_L = \phi_1 = \phi_2, \tag{11}$$

where subscripts L, R and V in this paper denote the values related to the left ridge, the right ridge and the critical-velocity ridge, respectively.

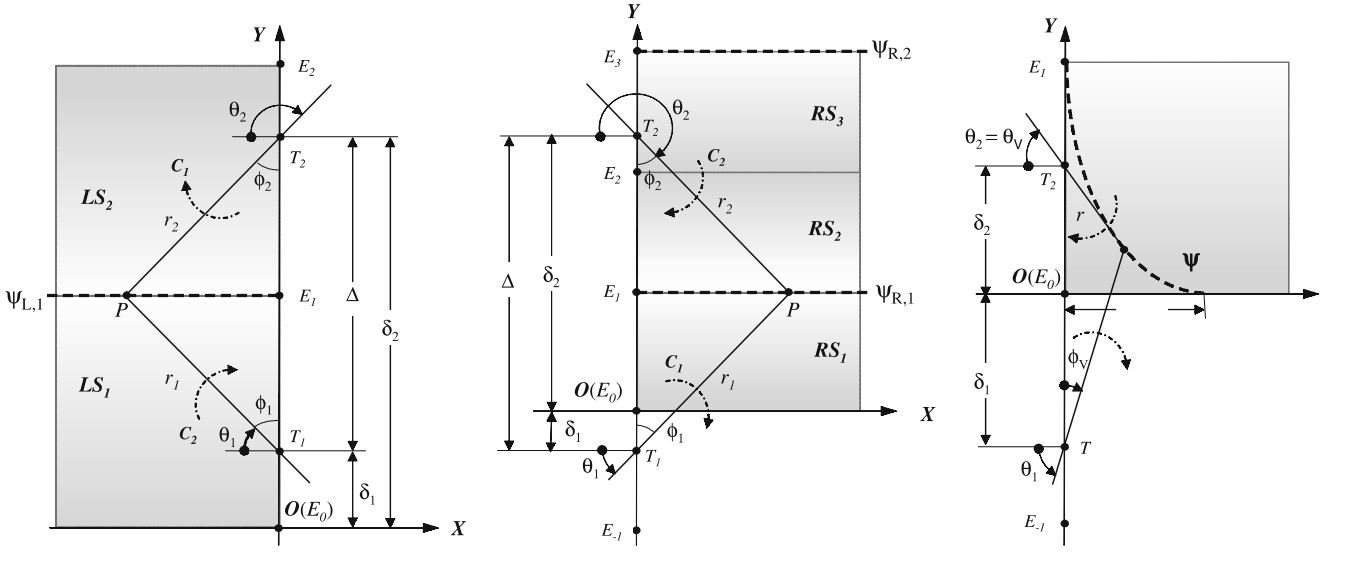

(a) Left-half ridge (b) Right-half ridge (c) Lower critical-velocity ridge

Fig. 6. Generation mechanisms of ridges

It is also apparent that the triangle PT_1T_2 is an isosceles triangle (Fig. 6a). So the effective cutter radius of the left ridge, $R_{eff,L}$ is expressed as

$$R_{eff,L} = \frac{\Delta}{2}\sec\phi_L = f_t\left(\frac{\phi_L}{\pi}\right)\sec\phi_L$$
$$\text{for } 0 \le R_{eff,L} \le R \text{ and } 0 \le \phi_L\,, \tag{12}$$

where Δ is the length of $\overline{T_1T_2}$, which is calculated as follows:

$$\Delta = \delta_2 - \delta_1 = f_t\left(\frac{\theta_2}{\pi}\right) - f_t\left(\frac{\theta_1}{\pi}\right)$$
$$= f_t\left(\frac{\phi_1+\phi_2}{\pi}\right) = 2f_t\left(\frac{\phi_L}{\pi}\right)\,. \tag{13}$$

As shown, $R_{eff,L}$ is given as a function of the feed per tooth, f_t, and the parameter ϕ_L denotes the rotation angle of the cutting edge.

Finally, the equation of the left ridge, ψ_L, which represents the heights of the cut remainder in the left plane of the machined surface, can be represented by the following parametric equation:

$$\psi_L = \begin{bmatrix} x_L \\ z_L \end{bmatrix} = \begin{bmatrix} -f_t\left(\frac{\phi_L}{\pi}\right)\tan\phi_L \\ H_L \end{bmatrix}\,, \tag{14}$$

where $H_L = R - \sqrt{R^2 - R_{eff,L}^2}$.

3.2.2 Right ridge (ψ_R)

The first right ridge, $\psi_{R,1}$, is the intersection line of the machined surfaces, RS_1 and RS_2, in Fig. 5. The generation mechanisms of RS_1 and RS_2 are described in Table 1. Similarly to the left ridge, the analytic equation of the right ridge, ψ_R, can be derived from the generation mechanism shown in Fig. 6b.

Just as in the previous case, the geometrical assumptions can be written as

$$R_{eff,R} = r_1 = r_2$$
$$\phi_R = \phi_1 = \phi_2\,. \tag{15}$$

The length, Δ, in Fig. 6b is calculated as follows:

$$\Delta = \delta_2 + \delta_1 = f_t\left(\frac{\theta_2}{\pi}\right) + f_t\left(\frac{\theta_1}{\pi}\right)$$
$$= f_t\left(\frac{2\pi - (\phi_1+\phi_2)}{\pi}\right) = 2f_t\left(1 - \frac{\phi_R}{\pi}\right)\,. \tag{16}$$

From Eqs. 15 and 16 the equation of effective cutter radius, $R_{eff,R}$, can be obtained by

$$R_{eff,R} = \frac{\Delta}{2}\sec\phi_R = f_t\left(1 - \frac{\phi_R}{\pi}\right)\sec\phi_R$$
$$\text{for } 0 \le R_{eff,R} \le R \text{ and } 0 \le \phi_R\,. \tag{17}$$

The equation of the right ridge, ψ_R, can therefore be expressed in the following form:

$$\psi_R = \begin{bmatrix} x_R \\ z_R \end{bmatrix} = \begin{bmatrix} f_t\left(1 - \frac{\phi_R}{\pi}\right)\tan\phi_R \\ H_R \end{bmatrix}\,, \tag{18}$$

where $H_R = R - \sqrt{R^2 - R_{eff,R}^2}$.

3.2.3 Critical-velocity ridge (ψ_V)

The critical-velocity ridge is formed in the regions where the velocity of translational movement of the cutter is faster than the rotational velocity. The first lower critical-velocity ridge, $\psi_{V,L1}$, is the intersection line of the machined surface RS_1 and the cutting edge plane Γ, which rotates while the cutter moves from E_0 to E_1.

Figure 6c is a schematic diagram of the generation mechanism of $\psi_{V,L1}$. The geometrical constraints at point $P(x_p, y_p, z_p)$ can be written as

$$x_p = r_1\sin\phi_V = r_2\cos\theta_V$$
$$y_p = r_1\cos\phi_V - f_t\left(\frac{1}{2} - \frac{\phi_V}{\pi}\right) = -r_2\sin\theta_V + f_t\left(\frac{\theta_V}{\pi}\right)\,. \tag{19}$$

Since the ridge is tangent to the cutting edge plane Γ at P, the relationship of r_2 and θ_V is given by

$$\frac{\partial y_p/\partial\theta_V}{\partial x_p/\partial\theta_V} = \frac{-r_2\cos\theta_V + \frac{f_t}{\pi}}{-r_2\sin\theta_V} = -\tan\theta_V\,. \tag{20}$$

Rearranging Eq. 20, r_2 can be written as follows:

$$r_2 = \frac{f_t}{\pi}\cos\theta_V\,. \tag{21}$$

By combining Eqs. 19 and 21, the effective cutter radius of the critical-velocity ridge, $R_{eff,V}$, is obtained by

$$R_{eff,V} = r_1 = \frac{f_t}{\pi}\frac{\cos^2\theta_V}{\sin\phi_V}\,. \tag{22}$$

The relationship of θ_V and ϕ_V can be expressed as

$$\phi_V - \theta_V + \cos^2\theta_V\cot\phi_V + \sin\theta_V\cos\theta_V = \frac{\pi}{2}$$
$$\text{for } 0 \le \phi_V, \theta_V \le \pi/2\,. \tag{23}$$

By solving Eq. 23 using a numerical method, $R_{eff,V}$ can be calculated by Eq. 22. Moreover, Eq. 22 shows that the critical-velocity ridge is created by cutting edges of radii which are smaller than f_t/π. Hence the width of the critical-velocity ridge in cross-feed direction, κ_V, is f_t/π.

Consequently, the analytic equation of the lower critical velocity ridge, $\psi_{V,L}$, can be written as follows:

$$\psi_{\mathbf{V},L} = \begin{bmatrix} x_{V,L} \\ y_{V,L} \\ z_{V,L} \end{bmatrix} = \begin{bmatrix} \frac{f_t}{\pi}\cos^2\theta_V \\ \frac{f_t}{\pi}(\theta_V - \sin\theta_V\cos\theta_V) \\ H_V \end{bmatrix}$$
$$\text{for } 0 \le \theta_V \le \pi/2\,, \tag{24}$$

where $H_V = R - \sqrt{R^2 - R_{eff,V}^2}$.

The equation of the upper critical velocity ridge, $\psi_{V,U}$, can be expressed as Eq. 25 because it is geometrically symmetric to $\psi_{V,L}$:

$$\psi_{\mathbf{V},U} = \begin{bmatrix} x_{V,U} \\ y_{V,U} \\ z_{V,U} \end{bmatrix} = \begin{bmatrix} \frac{f_t}{\pi} \cos^2 \theta_V \\ f_t - \frac{f_t}{\pi}(\theta_V - \sin\theta_V \cos\theta_V) \\ H_V \end{bmatrix}$$

for $0 \le \theta_V \le \pi/2$. (25)

4 Predicted results

Figure 7a shows the reconstructed characteristic lines of the cut remainder predicted using Eqs. 14, 18, 24 and 25 for the cutting condition of a tool radius of 5 mm and a feed per tooth of 0.5 mm/tooth.

In Fig. 7b, the profiles of the cut remainder, in section Π predicted by the proposed method, are compared with the profiles estimated by the Z-map method and the conventional roughness model. As shown, the left ridge and the right ridge predicted by the ridge method coincide very well with the profiles calculated by the simulation method, demonstrating the validity of the approach described in this paper.

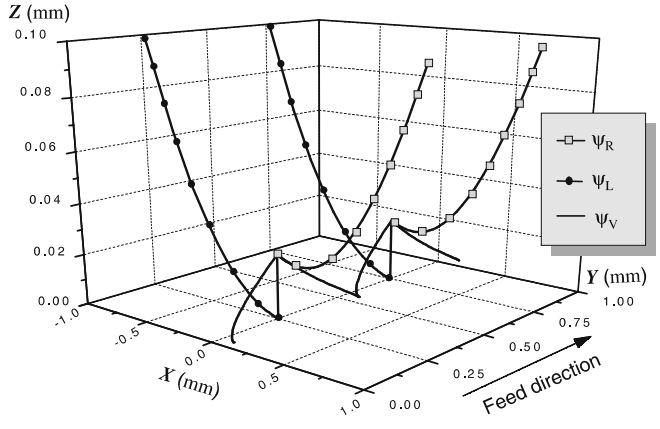

(a) Predicted trajectories of ridges

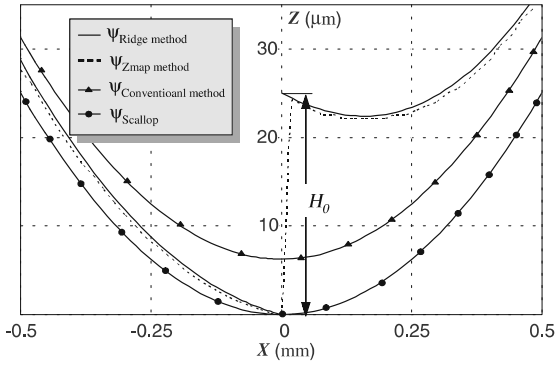

(b) Expected profiles of cut remainder (in maximum cut remainder section)

Fig. 7. Analysis of cut remainder by ridge method ($R = 5$ mm, $f_t = 0.5$ mm)

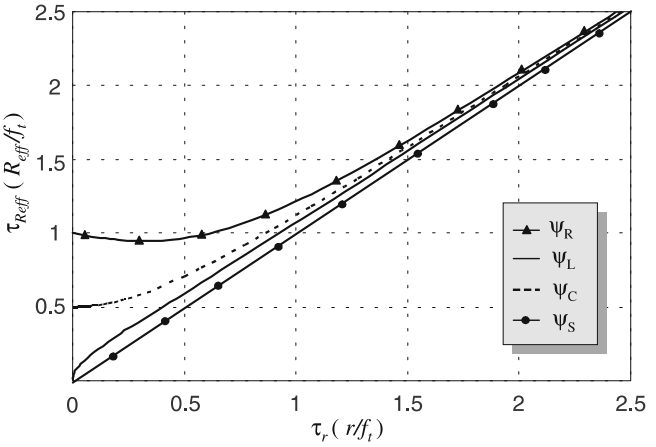

Fig. 8. Comparison of effective cutter radius (R_{eff})

The ridges in the maximum cut remainder section of this roughness model are discontinuous, and the maximum height of the cut remainder at the rotational center, H_0 can be obtained from Eq. 18:

$$H_0 = R - \sqrt{R^2 - f_t^2}\,. \tag{26}$$

Figure 8 shows the relationship between the effective cutter radius, R_{eff}, and the radius of the cutting edge, r. From Fig. 8 it can be seen that the value evaluated by the conventional roughness model becomes close to the value of the ridge method as the ratio τ_r increases. Therefore, if the feedrate is small relative to the path interval, the conventional roughness model is able to estimate the surface roughness and texture properly. However, the theoretical roughness in highly efficient cutting conditions cannot be predicted satisfactorily by the conventional roughness model.

5 Conclusions

In this study, a new approach, the *ridge method*, was proposed for the effective prediction of the geometrical roughness in the ball-end milling process. Theoretical analysis of a machined surface texture was performed on the basis of the disk-tool approximation model. The characteristic lines of cut remainder were defined as three types of ridges and their analytic equations were derived from the surface generation mechanism of the ball-end milling process. The equations of the ridges were given as functions of the tool radius, the feed per tooth and the rotation angle of the cutting edges. The agreement between the results predicted by the proposed method and the values calculated by the simulation method shows that the analytic equations presented in this paper are useful for evaluating the geometrical machining error of ball-end milling process.

In part II of this paper, the surface roughness and the shapes of surface texture are investigated using a suggested method considering the influence of feedrate, path interval and cutting modes (unidirectional mode and bidirectional mode), and an experimental verification is carried out.

References

1. Smith S, Tlusty J (1991) An overview of modeling and simulation of milling process. ASME J Eng Ind 113(2):169–175
2. Tlusty J (1978) Analysis of state of research in cutting dynamics. Ann CIRP 27(2):583–589
3. Zhang GM, Kapper SG (1991) Dynamics generation of machined surfaces, Part 1: Description of a random excitation system. ASME J Eng Ind 113(2):137–144
4. Schulz H (1991) High-speed milling of dies and moulds – cutting conditions and technology. Ann CIRP 44(1):35–38
5. Shatla M, Altan T (2000) Analytical modeling of drilling and ball end milling. J Mater Process Technol 98(1):125–133
6. Yang MY, Park HD (1991) The prediction of cutting force in ball-end milling. Int J Mach Tools Manuf 31(1):45–54
7. Feng HY, Menq CH (1994) The prediction of cutting forces in ball-end milling process. I: Model formulation and model building process. Int J Mach Tools Manuf 34(4):697–710
8. Feng HY, Menq CH (1994) The prediction of cutting forces in ball-end milling process. II: Cut geometry analysis and model verification. Int J Mach Tools Manuf 34(4):711–720
9. Lazoglu I, Liang SY (1997) An improved analytic modeling of force system in ball-end milling. Manuf Sci Eng 2:135–141. Also in: Proceedings of the 1997 ASME international mechanical engineering congress and exposition, Dallas, 12–16 November 1997
10. Feng HY, Menq CH (1996) A flexible ball-end milling system model for cutting force and machining error prediction. ASME J Manuf Sci Eng 118(3):461–469
11. Ikua BW, Tanaka H, Obata F, Sakamoto S, Kishi T, Ishii T (2001) Prediction of cutting forces and machining error in ball end milling of curved surface. I: Theoretical analysis. J Int Soc Precis Eng Nanotechnol 25(3):266–273
12. Ikua BW, Tanaka H, Obata F, Sakamoto S, Kishi T, Ishii T (2002) Prediction of cutting forces and machining error in ball end milling of curved surface. II: Experimental verification. J Int Soc Precis Eng Nanotechnol 26(1):69–82
13. Kanata H, Obata F, Ikua BW, Sakamoto S, Ashimori M (1999) Cutting forces and machining error in ball end milling of inclined flat surfaces. Int J Jpn Soc Precis Eng 33(3):319–325
14. Loney GC, Ozsoy TM (1987) NC machining of free form surfaces. Comput Aided Des 19(2):85–90
15. Vickers GW, Quan KW (1989) Ball-mills versus end-mills for curved surface machining. ASME J Eng Ind 111(2):22–26
16. Choi BK, Jerard RB (1998) Scupltured surface machining – theory and applications. Kluwer, Dordrecht
17. Miyazawa S, Takada K (1981) Micro milling of three-dimensional surface. J Jpn Soc Precis Eng 47(2):94–99 [in Japanese]
18. Naito K, Ogo K, Konaga T, Abe T, Kanda K, Matusouka K (1994) Development of ball end milling for fine high-efficiency finishing. Int J Jpn Soc Precis Eng 28(2):105–110
19. Kim BH, Chu CN (1994) Effect of cutter mark on surface roughness and scallop height in sculptured surface machining. Comput Aided Des 26(3):179–188
20. Kim BH, Chu CN (1999) Texture prediction of milled surface using texture superposition method. Comput Aided Des 31(3): 485–484
21. Koreta N, Egawa T, Kuroda M, Watanabe K, Ii Y (1993) Analysis of surface roughness generation by ball end mill machining. J Jpn Soc Precis Eng 59(9):129–134 [in Japanese]